Influence of Adsorbates on the Electronic Structure, Bond Strain, and Thermal Properties of an Alumina-Supported Pt Catalyst

Matthew W. Small,[†] Sergio I. Sanchez,[†] Nebojsa S. Marinkovic,[‡] Anatoly I. Frenkel,[§,*] and Ralph G. Nuzzo[†,*]

[†]School of Chemical Sciences and the Fredrick Seitz Materials Research Laboratory, University of Illinois, Urbana, Illinois 6180, United States, [‡]Center for Catalytic Science & Technology, Delaware University, Newark, Delaware 19716, United States, and [§]Department of Physics, Yeshiva University, New York, New York 10016, United States

ABSTRACT

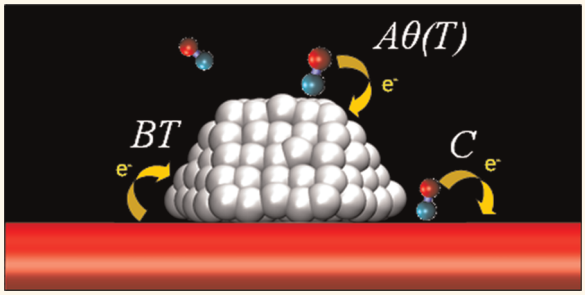

We describe the results of an X-ray absorption spectroscopy (XAS) study of adsorbate and temperature-dependent alterations of the atomic level structure of a prototypical, noble metal hydrogenation and reforming catalyst: ~1.0 nm Pt clusters supported on gamma alumina (Pt/γ-Al_2O_3). This work demonstrates that the metal−metal (M−M) bonding in these small clusters is responsive to the presence of adsorbates, exhibiting pronounced coverage-dependent strains in the clusters' M−M bonding, with concomitant modifications of their electronic structures. Hydrogen and CO adsorbates demonstrate coverage-dependent bonding that leads to relaxation of the M−M bond strains within the clusters. These influences are partially compensated, and variably mediated, by the temperature-dependent electronic perturbations that arise from cluster−support and adsorbate−support interactions. Taken together, the data reveal a strikingly fluxional system with implications for understanding the energetics of catalysis. We estimate that a 9.1 ± 1.1 kJ/mol strain exists for these clusters under H_2 and that this strain increases to 12.8 ± 1.7 kJ/mol under CO. This change in the energy of the particle is in addition to the different heats of adsorption for each gas (64 ± 3 and 126 ± 2 kJ/mol for H_2 and CO, respectively).

KEYWORDS: X-ray absorption spectroscopy · nanoparticle · platinum · γ-Al_2O_3 · catalyst · hydrogen · carbon monoxide

Investigations of heterogeneous catalytic efficacies are commonly made by monitoring changes in catalyst performance resulting from changes made to macroscopic experimental variables. These variables commonly include temperature, pressure, feedstock ratios, support and promoter compositions, and dispersion.[1−7] Such classical rate/property correlations frequently contain the implicit assumption that the catalyst's metal-bonding structure remains static despite changing conditions. While *a priori* this might seem reasonable, recent studies have begun to show that catalysts dynamically evolve by interacting with their environment through unique combinations of bond strain and electronic exchange.[8−12] The roles of both factors are reflected in several features: the binding strengths of adsorbates; facet-dependent turnover rates; and adsorbate-driven structural changes.[10,12,13]

Although Pt/γ-Al_2O_3 is perhaps one of the most prototypical examples of an industrially important heterogeneous catalyst, and thus the subject of numerous studies,[14−24] many aspects of its atomic structure and dynamical features under operating conditions remain poorly understood. This deficiency derives in part from the complexity of the system under realistic operating conditions and the limitations of experimental and theoretical methods of characterization in accommodating them. Even so, progress in each of the latter has begun to accelerate, albeit along generally independent paths.[19,20,25−28] There remains, as a result, a general need to provide experimental measurements that probe the limited length and time-scales accessible to theory. This study addresses questions of catalyst structure and dynamics that are motivated by this larger need.

In this study, we use the spectroscopic capabilities of XAS to build a deeper understanding of how supported Pt catalysts evolve in high-pressure/high-temperature environments by examining nanoscale, supported clusters under different partial pressures of H_2 and CO with changing temperature. Changes in the electronic and M−M bonding structures are monitored using the X-ray absorption near-edge structure (XANES) and the extended X-ray absorption

* Address correspondence to r-nuzzo@illinois.edu, anatoly.frenkel@yu.edu.

Received for review April 6, 2012 and accepted May 9, 2012.

Published online May 09, 2012
10.1021/nn3015322

fine structure (EXAFS), respectively. These data serve to elucidate underlying features of atomic structure *via* specific bonding-centric attributes, specifically, the first nearest neighbor (1NN) coordination number (CN); bond distance (R); the dynamical and static contributions to the mean square disorder (the EXAFS Debye–Waller factor, σ^2); and the correlated changes in electronic structure revealed by XANES. We examined the response of these features in the Pt/γ-Al_2O_3 system under steady state conditions using isobars and isotherms to explore various adsorbate coverages. In this way, we were able to characterize heretofore poorly understood contributions to the Pt clusters' bonding, including atomic strains and the system's electronic structure, which are both coverage- and temperature-dependent. These data affirm the predictions of a model that accounts for the anisotropic evolution of dynamic and static strains in terms of atomic (quasi-elastic) deformation energies.

RESULTS

Despite the frequently used, simplifying assumption that catalysts have ideal crystal structures,[29−32] the representative aberration-corrected scanning transmission electron microscope (C_s-STEM) data of Figure 1 clearly show that this is not the case for very small Pt nanoparticles supported on γ-Al_2O_3. Although the structure of an ideal, hemispherical truncated cuboctahedron, is a commonly used model for Pt/γ-Al_2O_3 and is used for interpreting many experimental observations,[8,29,33,34] such perfect structures in this size range are exceedingly rare. It is interesting to note that clusters in this size range all embed substantial static disorder, whether synthesized by colloidal/wet chemical methods or the impregnation/reduction method used here.[35] The supported clusters examined in this work thus accord well in this respect with the properties of nanoparticles of the same average size and distribution in cluster width created using micellar methodologies.[35−37]

The disordered structures evidenced in Figure 1 indicate that the clusters possess a large amount of embedded M–M bond strain. Observations of intracluster strain are not new, with surface relaxation being one of the best known examples.[9,31,38−41] The importance of the support's mediating role in developing specific attributes of strain and anisotropies in crystal truncations, however, has only recently begun to be understood.[8,42−46] On the basis of analogies with the properties of larger single-crystal surfaces,[7,47−50] one expects that many features of catalysts' M–M bonding structures will be modified under operating conditions. Strain profiles, for example, may be altered by impurities, defects, changing temperature, and the bonding of the cluster to specific support structures and/or adsorbate species. We also note that the strain

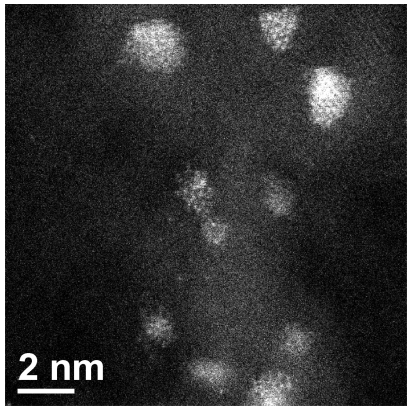

Figure 1. Aberration-corrected STEM image of Pt/γ-Al_2O_3.

may change with temperature and thus the assumption, commonly used in EXAFS analysis, that the static disorder contribution to σ^2 is constant should be critically examined in each particular case.

The data in Figures 2–4 demonstrate how the Pt/γ-Al_2O_3 system changes under a variety of conditions. Because there are many factors at play in these experiments, it is helpful to think how a generalized model system might behave under similar conditions and use it to help identify the most important factors that might affect the observed results. As more electron density is donated to the cluster at a fixed temperature, the Pt–Pt bond distance will increase.[18,26,51,52] Such effects can be caused by an increase in the number of electron-donating species bonded to the Pt and/or an increase in the amount of electron donation coming from interactions with the support. The coverage-dependent case is mediated most directly by both the partial pressure of the adsorbing species and the temperature of the system, while the impacts due to the support interaction will depend (at least for simple cases) almost solely on the temperature.[28] Similarly, adsorbates are known to induce (re)structuring of metal surfaces[47−49] and nanoparticle structures[13,53,54] so a change in the Pt–Pt coordination and cluster order may exist and depend on both the type of adsorbate and its partial pressure. If this (re)structuring indeed exists, it should also decay as the partial pressure decreases and at higher temperatures where thermally induced fluctuations and lower adsorbate coverages act to obscure features related to bond ordering and (atomic) structural relaxation.

The R_{Pt-Pt} and static component of the σ_{Pt}^2 data obtained from EXAFS analysis allows us to monitor both the nature and magnitude of changes in the average intraparticle strains that are present in a sample of Pt/γ-Al_2O_3. We note that these strains are inhomogeneously distributed in clusters of this type, with the surfaces and other low CN occupancies being impacted the most profoundly.[31] Since EXAFS probes all types of bonds, our results are inherently averaged over the entire ensemble of bonds present in a set of

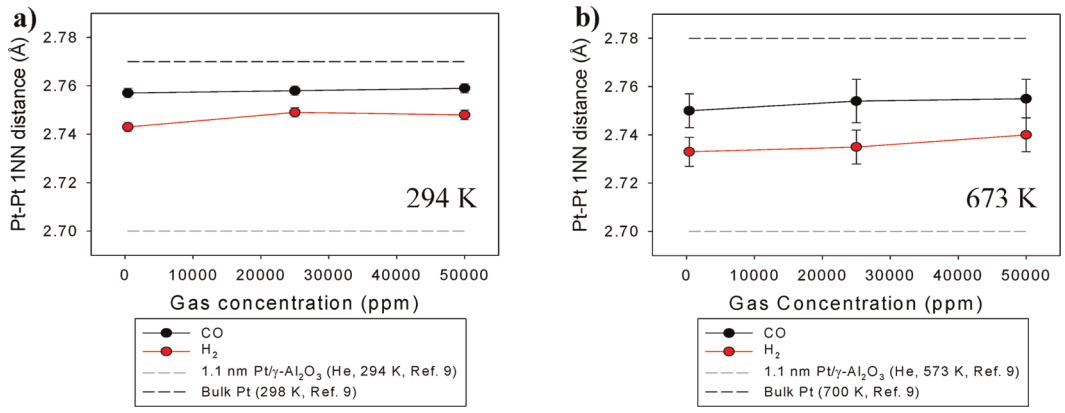

Figure 2. Pt−Pt 1NN distances at (a) 294 and (b) 673 K for different partial pressures of CO and H_2. Dashed lines indicate the values expected for bulk Pt (black) and values previously reported[9] for 1.1 nm Pt/γ-Al_2O_3 under He (gray).

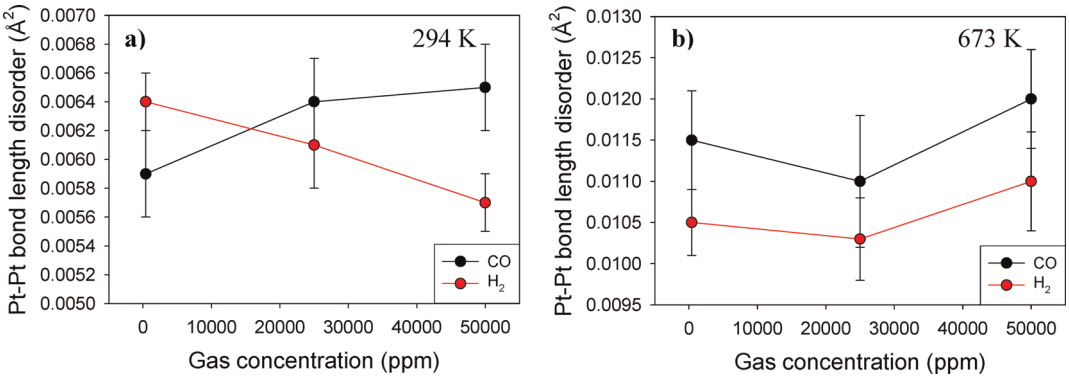

Figure 3. Pt−Pt bond length disorder (σ_{Pt}^2) values at (a) 294 and (b) 673 K for different partial pressures of CO and H_2.

clusters and, hence, underestimate the bond length perturbations due to the adsorbate and support interactions. The results plotted in Figure 2 show that the Pt−Pt bond lengths, R_{Pt-Pt}, for Pt/γ-Al_2O_3 under H_2 and CO atmospheres exhibit strong size, temperature, and partial pressure dependencies. Comparing Figure 2a,b, contractions of R_{Pt-Pt} relative to bulk Pt are evident with increasing temperature and agree with trends described in other reports.[9,18,51] They are expanded, however, relative to values previously reported[9] for a similarly sized, adsorbate-free Pt/γ-Al_2O_3 system, indicating the importance of adsorbate interactions as a mechanism for lifting surface relaxations. Of the two gases, CO elicits longer Pt−Pt bond lengths than does H at all comparable partial pressures and temperatures. Although within the uncertainties, each adsorbate also appears to progressively lift the initial bond relaxations with increasing partial pressure at a given temperature. The longer Pt−Pt bond lengths seen under CO make intuitive sense since CO has a larger heat of adsorption[55,56] and is known to be the more strongly electron-donating adsorbate species.[57,58] Unfortunately, this difference is entwined with the possibility that the state of the support is different for each adsorbate (*e.g.*, it is known that heating in a H_2-free environment leads to a so-called "dehydroxylation" of the support) and because temperature and coverage effects are intimately convolved.

Changes in the particle structure are also reflected by σ_{Pt}^2 (Figure 3), which is correlated to both the static and dynamic bond disorder present in the system. In the data in Figure 3a, for example, we see that the amount of disorder under CO and H_2 exhibit diverging, pressure-dependent trends. For CO, there is a tendency toward increasing disorder (deduced by the increasing magnitude of σ_{Pt}^2) as the partial pressure of CO increases, whereas the Pt−Pt bonding becomes increasingly ordered with increasing partial pressure of H_2. At higher temperatures (Figure 3b), there appears to be only a weak (if any) adsorbate pressure dependence on the ordering of the Pt particles. The CO data, despite having overlapping uncertainties with the H_2 data, consistently exhibit increased disorder for all pressures. The larger body of data strongly indicates that CO is forcing a more disordered state (*i.e.*, a broader distribution of M−M bond distances) even at higher temperatures. Since CO is a stronger electron donor than H_2, it should relieve surface relaxation more efficiently, as is evidenced in Figure 2. If the bond disorder was

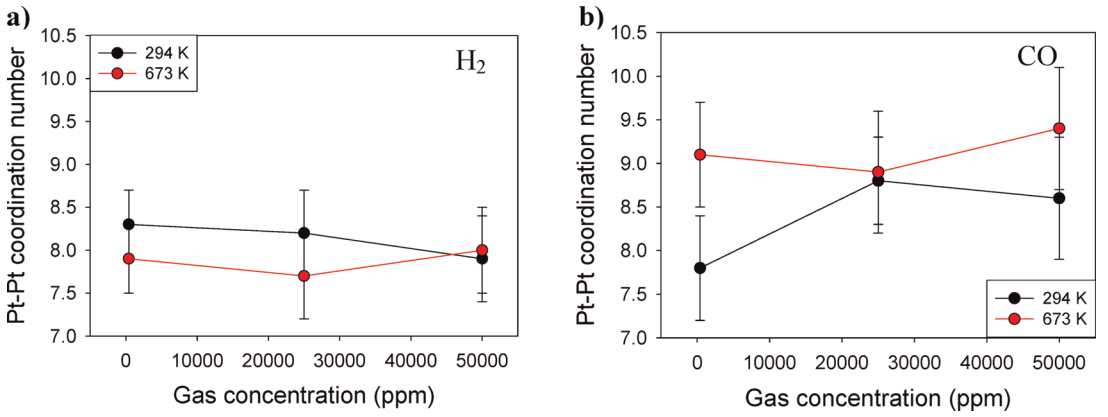

Figure 4. Pt−Pt 1NN coordination numbers for the lowest and highest temperatures studied, plotted as a function of partial pressure: (a) H_2/He and (b) CO/He.

completely attributable to surface relaxation, CO should lead to a more ordered state with increasing partial pressure. Since this is not reflected in a simple way in the σ_{Pt}^2 data, this behavior must be caused by some other impact that attends its bonding. The data, and discussions that follow, develop this latter aspect more quantitatively by examining aspects of strain and cluster shape.

The most explicit manifestation of bond strain differences between the two adsorbate environments is evident in the measured Pt−Pt CNs of the Pt clusters (Figure 4). The CNs found under hydrogen are always lower than those evidenced in a CO environment and exhibit only weak pressure and temperature dependencies. Carbon monoxide elicits quite different behaviors in these same clusters—impacts that, due to their reversibility, cannot arise as a consequence of sintering. In the presence of CO, the Pt−Pt coordination increases relative to H_2 and has an unusual temperature dependence in that the Pt−Pt coordination number is higher for the highest temperature at all partial pressures. We note that application of our model, which allows varying CNs, to bulk Pt measured at various temperatures showed only a minor tendency toward decreasing CNs that was well within experimental uncertainties for bulk Pt. Such a trend is in contrast to the CO data wherein the CNs of the Pt increase appreciably with temperature. Interestingly, and in a way qualitatively similar to H_2, only a weak dependence on partial pressure is found. The dynamical underpinnings of this behavior are established unambiguously by the fact that the system could be cycled with full reversibility over all partial pressures. Despite the uncertainties ascribed to the CN fits, this strongly suggests that complex mechanistic factors are at work here. These may range from shape change phenomena induced by adsorption[13,59] to more complex changes originating from the amount of support wetting. Other authors have described a cluster-shape-change behavior for CO adsorption on unsupported Au nanoclusters, suggesting that CO adsorption induces a flattening of the particle.[59] Spreading of the Pt cluster upon CO adsorption also agrees with Campbell's observation[60] that if the energy difference between the adsorbate−metal and adsorbate−support bonding is large enough to overcome the difference in the M−M and M−support bonding, particle flattening will occur. The trends evidenced here, though for a supported system, also seem to point toward a structure that flattens and more strongly "wets" the substrate as a consequence of exposure to CO. This is similar to the theoretical predictions of Hu *et al.* that modeled an increase in electron donation to Pt_{13} and Pd_{13} clusters on γ-Al_2O_3 *via* the effects of increasing support hydroxylation.[34] We discuss the concept of support wetting in more detail below.

While understanding the order and morphological evolution of Pt clusters under different environments is beneficial, a more thorough understanding of how the catalytic activity is affected also requires knowledge of changes to the clusters' electronic structures. One means of monitoring the relative change in features of electronic structure between conditions is through their near-edge difference spectra (the ΔXANES). Such data are shown in Figure 5. As expected, increasing the temperature and/or decreasing the partial pressure of the adsorbate gas leads to a smaller change for H_2 relative to the reference value (400 ppm, 673 K) for both gases. A more quantitative means of comparison is provided by plotting the absolute, integrated area ($S(T,P)$) of each ΔXANES spectrum (Figure 6). Interestingly, the resulting curves exhibit the behaviors expected for generic desorption curves at different partial pressures near the full and zero coverage limits for CO and H_2, respectively. There are some features that, initially, appear unusual for the CO data. The first is the presence of a nearly linear change in the integrated intensity with increasing temperature for all data even well below temperatures where this adsorbate partial pressure should be sufficient to saturate the Pt surface (*i.e.*, coverage ~1.0). The second somewhat odd feature is the offsets present even at the lowest

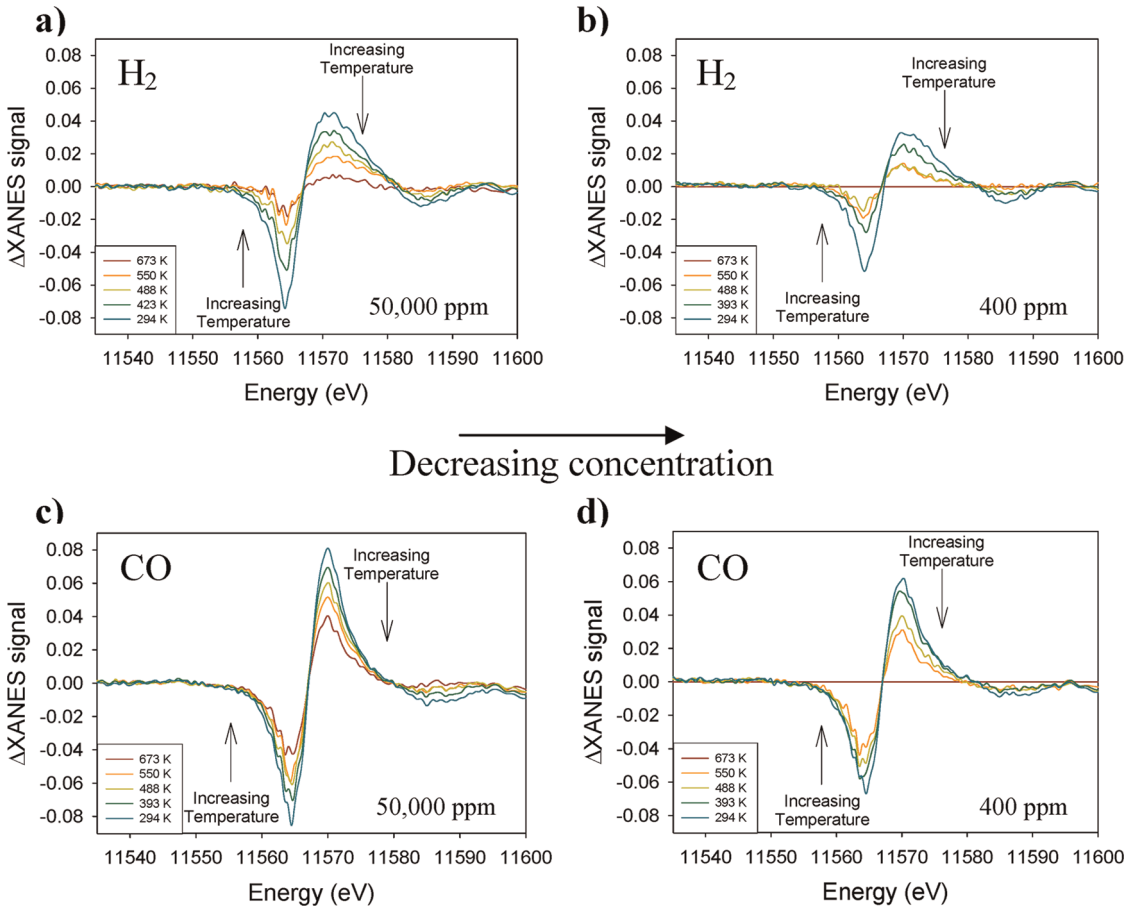

Figure 5. ΔXANES spectra for H_2 (a,b) and CO (c,d) using 400 ppm of each gas at 673 K as a reference.

temperature for the different CO pressures, where the cluster surface should be saturated with adsorbate. The predictions of a theoretical model (shown here as lines plotted in Figure 6, *vide infra*) explaining the sources of these changes, and their importance to the system, are discussed below.

DISCUSSION

The efficacy of a catalyst is generally thought to result as a consequence of the combined influences of their electronic and atomic structural characteristics.[48,49] When these factors work synergistically, low energy pathways for a reaction can be engendered. Many approaches have been used to alter catalysts in the hope of improving their performance including changing the support material,[10,49,61] doping,[62,63] alloying,[8,12,53,64,65] facet/defect modifications,[5,30,32] and crystallographic anisotropy[32,49] to name a few. Judicious manipulation of these attributes has allowed for some measure of catalyst tailoring, creating structures that favor reactant adsorption and/or product desorption.

Some forms of the modifications seen in catalyst motifs relative to the bulk metals are innate to nanoscale systems. For example, the cluster structure in many cases can exhibit significant structural relaxation of surface atoms toward the cluster core. This results in an average bond length that is shortened with a weighting based on the population of surface atoms and other low coordination number sites (*e.g.*, vertices at the support interface).[31,38] Presenting data reported for bulk and 1.1 nm Pt/γ-Al_2O_3 under He[9] in juxtaposition to our data (Figure 2), we see that the presence of adsorbates relieves strains experienced in under-coordinated bonding environments. These strains, however, are neither completely dissipated (that would have resulted in bulk-like values of R_{Pt-Pt}) nor are they equivalent for CO and H_2 atmospheres. Exposure to CO leads to more bulk-like Pt−Pt bond distances than H_2, even at low partial pressures. This should be expected in light of the more strongly electron-donating character of CO and, concomitantly, its ability to relieve surface relaxation.[57,58]

An important feature of the structural fluxionality of Pt/γ-Al_2O_3 is revealed in the data presented in Figure 4, where the Pt−Pt CN under CO and H_2 is plotted at the highest and lowest temperatures tested. Notably, even though these plots show the same material, the Pt−Pt CN found for each gas is different. Thus, both the magnitude of the average bond length expansions seen and the geometric arrangement of atoms, as is required to induce changes in the CN of the magnitude

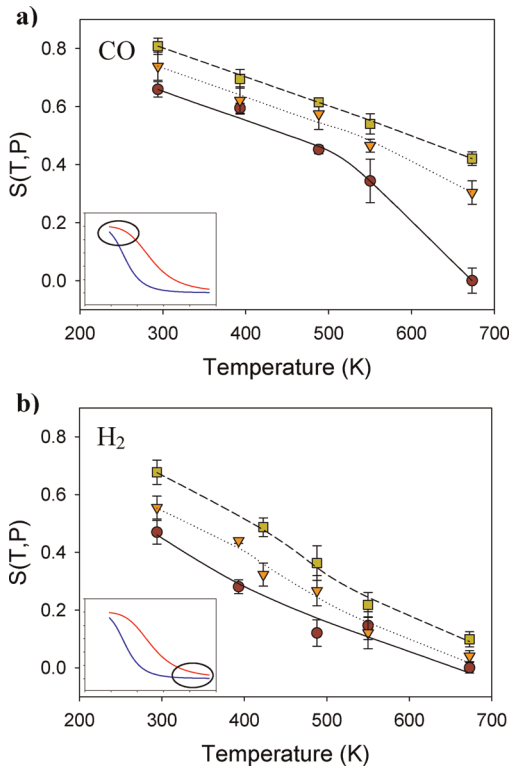

Figure 6. Plot of the integrated intensity obtained from the (a) CO and (b) H_2 ΔXANES. The different partial pressures are 400 ppm (circles), 25 000 ppm (triangles), and 50 000 ppm (squares). The solid lines are the lines of best fit obtained using eq 8. The insets show the general shape of a desorption curve (coverage *versus* temperature) derived using the Langmuir approximation and indicate (oval) the desorption region circled appropriate for the designated gas.

observed, show that the two cases are quite distinct. Aspects of the mechanism(s) involved are clearly subject to the influence of the adsorbate−metal bond strength (which is larger for CO), but it also remains a distinct prospect that differences in the metal−support interactions in each case (see below) play a significant role. Expansion toward more bulk-like Pt−Pt values, however, remains limited by the need to minimize the surface energy of the cluster and the interfacial strains induced by the γ-Al_2O_3 support.[8,42]

The modifications of bond strains induced by adsorbing species are also evidenced in the systematic trends of the σ_{Pt}^2 values under different isobaric and isothermal conditions. At 294 K, Pt/γ-Al_2O_3 under CO and H_2 takes on diverging trends with increasing partial pressures and, thus, coverage. Under CO, the disorder in the system increases with increasing partial pressure, whereas the disorder decreases for H_2. Since CO and H are known to have multiple binding sites on Pt,[49,66,67] one possible explanation for the observed behavior is that the relative occupancy of the binding sites is changing with the partial pressure of each gas. Adsorption of additional hydrogen, for example, would result in increasing electron donation to the Pt clusters and an increase in the number of H atoms binding at bridge, atop, and three-fold sites. Since H_2 adsorption is dissociative on Pt and results in highly mobile H atoms,[67] any changes observed should be primarily from a decrease in the number of unsatisfied Pt bonds. In contrast, CO favors molecular adsorption in an atop configuration.[68] Although CO can also bind in different conformations, it also experiences significant lateral repulsions at high surface coverages.[47,68] Atomistic attempts to relieve these interactions may impact σ_{Pt}^2 and manifest as increasing disorder. Direct comparison of the data for each gas at higher temperatures is less straightforward because their different desorption rates will lead to very different limiting coverages over the range of partial pressures examined. Furthermore, any temperature-dependent behavior of the strain may be different for each isobar and will not allow separation of the static and dynamic contributions to the total bond length disorder. This can, however, be done at lower temperatures where the dynamic contribution is much smaller. As the surface coverage of each gas decreases the thermal vibrations of intracluster bonds become more important to the final system disorder. Indeed, the relatively constant disorder embedded within the clusters across all partial pressures of both gases at 673 K hints that at higher temperatures the dynamic contributions to the bond disorder are weighted to a far greater extent than adsorbate-induced restructuring. This raises what is perhaps the most important, albeit complex, question addressed in this work: How can one best characterize the highly fluxional attributes of adsorbate-mediated bond strains using only a local, temporally, and spatially averaging tool such as XAS? In the above case, we see limiting behaviors where the qualitative trends suggest a significant weighting of the adsorbate-determined bond strains within the low-temperature and high-coverage limits. Similarly, higher temperatures progressively overweigh these adsorbate contributions as the magnitude of the dynamical term in σ_{Pt}^2 increases. The larger data do speak to the nature of the bond strains present more quantitatively, however.

Using the approach of Frenkel *et al.*,[69] we estimate strain energies associated with σ_{Pt}^2. The time and configuration averaged deformation energy (U) per metal atom in a metal cluster, assuming only 1NN contributions, can be evaluated as

$$U = \frac{1}{2} Nk\sigma^2 \qquad (1)$$

Here N is the M−M coordination number; k is the force constant of the M−M bond; and σ^2 is the mean square bond length disorder. In the harmonic approximation, the force constant is $k = \mu\omega^2$, where $\mu = m/2$ is the reduced mass of the M−M bond, $\omega = k_B\Theta_E/\hbar$ is the Einstein frequency, $\hbar$ is Planck's constant, and Θ_E is the Einstein temperature. When static (temperature-independent)

TABLE 1. Calculated Strain Energies for Pt/γ-Al_2O_3 under Different Gaseous Environments

gas/pressure	*N*(Pt−Pt)	Θ_E (K)	σ^2 (Å^2)	σ_s^2 (Å^2)	*W* (kJ/mol)
100% He[a]	6.3(3)	226(7)	0.0075(2)	0.0045(2)	12.1(1.1)
400 ppm H_2/He	8.3(4)	226	0.0064(3)	0.0034(3)	12.0(1.4)
25000 ppm H_2/He	8.2(5)	226	0.0061(3)	0.0031(3)	10.9(1.4)
50000 ppm H_2/He	7.9(5)	226	0.0057(2)	0.0027(2)	9.1(1.1)
400 ppm CO/He	7.8(6)	226	0.0059(3)	0.0029(3)	9.7(1.4)
25000 ppm CO/He	8.8(5)	226	0.0064(3)	0.0034(3)	12.8(1.6)
50000 ppm CO/He	8.6(7)	226	0.0065(3)	0.0035(3)	12.8(1.7)

[a] Derived from a previous report[9] of 1.1 nm Pt/γ-Al_2O_3 under He.

strain is present, eq 1 can be written as the sum of two contributions: $U = V(T) + W$, where $V(T)$ arises due to dynamic vibrations, and W originates from the static disorder present in the system of interatomic bonds. These two terms can be separately evaluated by expressing σ^2 in terms of the dynamic and static terms (σ_d^2 and σ_s^2, respectively) of the EXAFS Debye−Waller factor:

$$\sigma^2 = \sigma_d^2 + \sigma_s^2 \quad (2)$$

The residual elastic strain energy due to the static disorder is then identifiable as simply

$$W = \frac{1}{2} Nk\sigma_s^2 \quad (3)$$

This provides a foundation to evaluate the strain energies associated with the H_2 and CO adsorbate systems studied in this work. We limit our analysis to the strain evidenced in the Pt clusters at room temperature because the higher coverage and smaller thermal contributions yielded higher data quality and will result in the largest adsorbate-induced strains. Also, as mentioned above, the separation between the static and dynamic components of the disorder is expected to be more complicated at higher temperatures. In order to separate the static and dynamic terms from the total disorder measured at room temperature for all gas concentrations, we adopted a perturbative approach. In this model, the clusters are described in terms of a perturbation by adsorbates relative to the underlying "zero coverage" cluster. Any adsorbate-specific surface bond relaxation will then be accompanied by a concomitant change in the strain energy, *W*. Since the typical values of *W* obtained here (Table 1) are a small fraction of typical cohesive energies (*e.g.*, the cohesive energy of Pt is ~5.8 kJ/mol),[70−73] the effect of the adsorbate-induced stress is only weakly related to the elastic constants associated with nonsurface atoms. For this reason, the Einstein temperatures and frequencies for both adsorbates (H and CO) and all partial pressures studied in this work are set to the value derived for the zero coverage case.[9] Sticking with idealized cases, this approximation also fixes both *k* and σ_d^2 for all samples. Therefore, this approximation relies on the internal cluster atoms experiencing similarly shaped, effective potential wells.

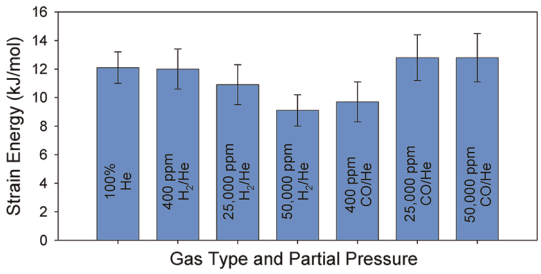

Figure 7. Graphical depiction of the strain data shown in Table 1.

The results of these calculations (Table 1) are shown graphically in Figure 7. Values of the elastic strain energy range from 9.1 to 12.8 kJ/mol, depending on the specific system conditions. Despite the fact that our estimates are derived from results that average over the entire cluster, we can use them as a lower bound for the strain energy of the more disordered surface layer. Even these underestimated strains are quite large and should be included in theories on nanoscale thermodynamics and reaction energetics.[74,75] We should also note that, besides its influence on the equilibrium configuration of ground state clusters, this static strain will likely play an important role in the thermal properties of particle−support−adsorbate systems.

The quantification of adsorbate-mediated strain energy in the Pt/γ-Al_2O_3 system provides new insights into the fundamental thermodynamic properties of this system that can be monitored using XAS. Figure 5 shows that the electronic characteristics of the system (as revealed in the ΔXANES data) actually (and unexpectedly) change monotonically with temperature and adsorbate concentration. Since the Pt L_3-edge white line intensity changes drawn out by the ΔXANES are directly related to Pt's d-state occupancy, there is a continuous reduction of the d-state population with increasing temperature and/or decreasing gas concentration. Plotting the absolute integrated area of these curves (Figure 6) shows that an increasing CO pressure leads to greater electronic changes at higher temperatures, whereas the H_2 data begin to converge with increasing temperature. Part of this differing behavior can be ascribed to near saturation (or zero) coverage of adsorbates present on the cluster surfaces (inset Figure 6a,b) under varying conditions, a dependency that is directly correlated with the gas partial pressure, temperature, and adsorbate bonding strength. Simple thermochemical kinetic calculations suggest, for example, that the coverage of H on Pt at 673 K is very low at the partial pressures we have examined.[76] Minimal changes in the absolute integrated intensity with varying partial pressure are therefore expected in this regime. In contrast, the stronger bonding of CO on Pt suggests that a significant coverage will still exist at 673 K (slightly above the desorption temperature) for

higher partial pressures but not for the lower partial pressures. Consequently, the absolute integrated intensities for high and low partial pressures of CO are expected to diverge in this case. In point of fact, the actual experimental observations embed additional temperature and partial pressure-dependent sensitivities.

The first important observation is that the ΔXANES for CO changes continuously with temperature, doing so even when the surface coverage should be completely saturated under 50 000 ppm CO. Since the coverage should be almost invariant under these conditions, this linear trend cannot be ascribed (as has been done in some cases reported in the literature)[18,77−79] directly to the number of adsorbed molecules. We believe that one mechanism involved here is actually related to the variation of the particle−support interactions with temperature. The sensitivity of the particle−support interaction to temperature can be attributed, in part, to the increased librational motion of clusters at elevated temperatures. Such factors in the structural dynamics of supported Pt catalysts have been treated both experimentally[9,18,51] and theoretically[28,46] in the recent literature and found to alter both the electronic and strain states present. We also note that a saturation coverage of the Pt surface with CO should also occur at 294 K for all partial pressures examined. The data of Figure 6 show that there exists a partial pressure-dependent vertical shift of the ΔXANES data. We ascribe this shift to the effects of the support−adsorbate interaction (*vide infra*). All of the trends seen in the ΔXANES signal can be empirically modeled in terms of contributions from a weighted composite of adsorbate−particle, particle−support, and adsorbate−support electronic interchanges using

$$S(T,P) = A\theta(T,P) + BT + C(P) \quad (4)$$

Here S is the integrated intensity of the ΔXANES signal; θ is coverage; and A, B, and C are the weighing of each component. In this equation, the first term on the right-hand side addresses electron donation from the species adsorbing on Pt and varies directly with coverage. The second term, BT, models the near-linear temperature dependence of the signal that we find in the data and ascribed to the temperature-mediated charge transfer between the particle and support. The final term on the right-hand side of eq 4 is the partial pressure-dependent offset observed in the experiments, which we believe can be attributed to alterations of the support, presumably *via* spillover, by the adsorbing gas molecules.

To provide quantitative analysis of the ΔXANES using eq 4, we describe the coverage-dependent contribution using a Langmuirian formalism

$$\theta(T,P) = \frac{(KP)^a}{1+(KP)^a} \quad (5)$$

where P is the pressure, K is the ratio of the adsorption and desorption equilibrium constants, and $a = 1$ or 0.5 for nondissociative or dissociative absorption, respectively. By expressing K as

$$K = A_0 e^{b/RT} \quad (6)$$

where A_0 is the ratio of exponential prefactors, b is the difference between the desorption and adsorption energies, and R is the ideal gas constant, we obtain

$$\theta(T,P) = \frac{1}{\alpha e^{-n/T}+1} \quad (7)$$

where $\alpha = 1/(A_0P)^a$ and $n = ab/R$. Thus eq 4 can be rewritten as

$$S(T,P) = \frac{A}{\alpha e^{-n/T}+1} + BT + C(P) \quad (8)$$

Since the adsorption of H_2 and CO on Pt are both nonactivated, the fit value of b is equivalent to the heat of adsorption, ΔH. To reduce the number of variables involved in the fit, we note that at full coverage (low T) eq 8 reduces to

$$S(T,P) = A + BT + C(P) \quad (9)$$

Therefore, a plot of S *versus* T, while maintaining full coverage (*e.g.*, 50 000 ppm CO), will provide values for B and $F(P) = A + C(P)$ *via* the slope and y-intercept, respectively. Rearranging eq 9, we obtain

$$S(T,P) = \frac{A}{\alpha e^{-n/T}+1} + BT + F(P) - A \quad (10)$$

We further assume that A_0 can be approximated by[15]

$$A_0 \sim \frac{h^3}{k_B(2\pi m k_B)^{3/2}} \times \frac{1}{T^{5/2}} \quad (11)$$

where k_B is Boltzmann's constant, h is Planck's constant, m is the mass of the adsorbing molecule, and T is the temperature. This means that A_0 will be on the order of $\sim 10^{-13}$ for CO and $\sim 10^{-11}$ for H_2 over the range of temperatures examined. If the system is near full coverage and the particle−support interaction with temperature (described by the coefficient B) is assumed independent of gas pressure, $F(P)$ will shift proportionally to the intensity offset observed at 294 K. Equivalently, the linear term will be vertically shifted for different partial pressures. Because we do not have measurements pertaining to a constant coverage of H_2 across all temperatures examined, we determined the B value from the CO curves.

Although these assumptions are idealized, and thus approximate, this ansatz leaves only two unknown values after substituting for theoretical and experimental values: A and n. Fitting n for all three pressures simultaneously while allowing A to vary permits estimation of ΔH for H_2 and CO adsorption. Alternatively, if possible changes in the extent of charge transfer caused by a significantly increased coverage/pressure

are ignored (*e.g.*, altered occupancy of less favorable binding sites), *A* can be treated as a common, partial pressure-independent variable for each adsorbate. Indeed, when *A* is allowed to vary with pressure, it shows a progressive trend toward increasing values for increasing H_2 pressure and an opposite trend for CO (Supporting Information). The resulting ΔH values using this fitting method are 64 ± 3 kJ/mol for H_2 and 126 ± 2 kJ/mol for CO. In the more constrained situtation, where *A* is treated as a common variable, a less satisfactory fit is produced. Even in this highly limited case the predicted ΔH values (61 ± 4 for H_2 and 131 ± 2 for CO) change only marginally.

The principle limitation of adopting a Langmuir isotherm to describe the coverage is that it inherently assumes a coverage-invariant ΔH. In general, heats of adsorption for adsorbates show an approximately linear dependence on coverage up to a monolayer.[15,27,80] For our system, we note that the CO coverage will vary over a maximal range of approximately 60−100%,[16] while the hydrogen will vary within an approximate range of 1−99%.[80] Therefore, the heats of adsorption derived by fitting the experimental data will represent average values over the coverage ranges examined. It should further be noted that our choice of reference means that the "coverage values" fit will range between 0 and 100% for both cases and are values based on our reference partial pressure and temperature. Nevertheless, the fitted coverage (Supporting Information) reproduces the behavior expected for constant pressure adsorbate coverage with increasing temperature (inset Figure 6). In addition to the coverage behavior, the values calculated for ΔH by fitting our equation fall nicely within the range of values reported in the literature for H_2 (∼50−83 kJ/mol)[56] and CO (∼100−140 kJ/mol)[56,81] on Pt, values that depend, variably, upon the technique used, the system (*e.g.*, (un)supported, bulk, *etc.*), the exposed facet(s)/CN of the Pt atoms and the adsorbate coverage. This analysis demonstrates that the XAS data, specifically the ΔXANES data, report on the electronic/structural features of these two chemisorption systems and provide a means to explicitly correlate these attributes to global thermodynamic values.

It is now clear that the particle−support interactions in the Pt/γ-Al_2O_3 system are significant and electronically complex but that fundamental aspects associated with charge exchange are strongly responsive to temperature. The current literature strongly supports the conclusion that these bonding interactions mediate a net charge flow to the Pt clusters from the support and may further embed an important role for oxygen atom vacancies in the oxide substrate as components of this bonding. Many features of the system—explicitly the anomalous thermal dependencies seen in the Pt−Pt bond lengths and properties of d-state occupancies that are implied by the ΔXANES intensities—argue strongly in support of this conclusion. At present, our ability to address these phenomena *via* quantitative theoretical models remains limited in important ways. Theory demonstrates nonvibrational (*e.g.*, librational) dynamics play a crucial role in shaping the thermal responses of Pt/γ-Al_2O_3, both in terms of anomalous XANES behaviors (*e.g.*, red shift) and the non-bulk-like temperature-dependent evolution of Pt−Pt bond distances. How this complex and markedly mesoscopic behavior might then lead to the systematic, essentially linear, dependencies of the ΔXANES intensities seen with temperature is presently not understood. We believe further work will be needed to assess the mechanism that might be involved.

We also note that the origins of the ΔXANES offsets seen in the isobaric temperature series presented in Figure 6 remain poorly understood. Clearly some form of support interaction/modification must be involved. We know with some certainty that the support differs in significant ways in the two adsorbate-based comparisons. In the work conducted in H_2 ambients, the formation of support-bonded H, bonding variably described as hydrogen spillover, hydroxylation, *etc.*, will alter the extent of support wetting by altering the particle−support interfacial energy.[22,34,61] The degree of surface hydroxylation is known to impact the binding energy of Pt to γ-Al_2O_3 as well as leading to structural rearrangements.[22,34] A changing number of hydroxide groups at the alumina surface should result in changes to the number of bonds to the Pt clusters and, thus, manifest as a shape change. Whatever its form, the high-temperature cycle in a CO environment will desorb this hydrogen and thus engenders a support phase with very different properties. Even so, and the quantitative differences not withstanding, the pressure-dependent offsets seen in Figure 6 are consistent with the expected behavior of an electron-donating species binding to the support. In such a case, the increasing electron density of the support will allow more electron density to be transferred to the cluster. This will manifest as an electronic shift consistent with increasing coverage even if the coverage remains static. Similarly, an increase in the electron transfer capabilities of the support will favor a greater wetting of the support. Still, the flattening of unsupported particles under CO has theoretically predicted and experimentally observed,[59] meaning that the reason(s) for an increase in the Pt−Pt CN with increasing temperature under CO but not H_2 remains a marked but poorly understood feature of the current data, one for which some form of theoretical description is urgently needed.

Finally, we note that the data also provide what we believe is the first description of how Pt−Pt bond strains respond to variable temperature and adsorbate partial pressure in Pt/γ-Al_2O_3 systems. The role of strain on the electronic structure and reactivity of Pt clusters was recently highlighted by Strasser *et al.*[12] It is important to note that our estimates of the strain energy are averaged over the cluster; that is to say that the strains experienced by specific atom sites in the Pt cluster surfaces could be significantly larger. Although the literature clearly establishes the validity of this latter hypothesis,[31] the energy content of this feature across the conditions examined has not yet been addressed. The present data suggest the impact of these strains is quite large. Indeed, the strain energy of each system can vary by almost 3 kJ/mol by merely changing the adsorbate partial pressure at room temperature. Further studies are in progress to more precisely quantify this latter aspect of the energetics and provide a rigorous set of benchmarks for address by theory.

CONCLUSION

Strain-driven electronic and morphological reconstructions of Pt clusters supported on γ-Al_2O_3 exhibit marked adsorbate and temperature dependencies. Monitoring these changes with XAS under steady state conditions, the contributions of adsorbates and temperature can be parsed, allowing for improved understanding and model development of the multicomponent interactions occurring. Our investigation shows how to extract both strain and thermodynamic information from XAS measurements and offers insight into the relative importance of adsorbate−particle, particle−support, and adsorbate−support interactions with changing temperature or pressure for Pt/γ-Al_2O_3. This indicates methods of tailoring catalytic activity and the relative magnitude of those changes on the final catalyst structure.

METHODS

Sample Preparation. A sample of 1 wt % Pt/γ-Al_2O_3 was prepared by impregnating 220 m^2/g γ-Al_2O_3 (Alfa Aesar) with $(NH_3)_4Pt(OH)_2$ (Sigma Aldrich). The sample was dried in air, and 110 mg was formed into a pellet at a pressure of 2.5 tons. The sample was further processed in the *in situ* XAS cell at beamline X19A at the National Synchrotron Light Source (NSLS) in Brookhaven National Laboratory, Upton, NY. Preparation of the sample consisted of equilibrating the pellet with 100% H_2 at room temperature for 30 min, raising the temperature to, and holding it at, 573 K for 1 h followed by cooling to room temperature in flowing H_2. Prior to experiments, the sample was re-reduced at the beamline by exposing it to 5% H_2/He at room temperature for 30 min and then raising the temperature to 723 K for 1 h.

Scanning Transmission Electron Microscopy Characterization. Scanning transmission electron microscopy (STEM) micrographs were used to characterize the size distribution of the particles. A small amount of the sample was suspended in ethanol and drop cast onto a copper grid coated with holey carbon (SPI Supplies) for analysis using a JEOL model 2010-F electron microscope operated at 200 kV in STEM mode. A survey of 300 particles yielded a particle size of 1.0 $\pm$ 0.2 nm (Supporting Information). Atomic resolution images were acquired using a JEOL 2200-FS operated at 200 kV in STEM mode.[82]

XAS Experimental Conditions. The Pt/γ-Al_2O_3 catalyst was examined under various partial pressures of both H_2 and CO at a series of temperatures using an *in situ* XAS cell. The temperatures for both gases were 673, 550, 488, 423, and 294 K (the 400 ppm H_2 was measured at 393 K instead of 423 K) and adjusted using feedback from a digitally controlled thermocouple. Three partial gas pressures were used for both H_2 and CO and were obtained by mixing He with 5% standards of the appropriate gas using Brooks flow controllers. The partial pressures reported are 50 000, 25 000, and 400 ppm of H_2 (or CO) in He, with a total pressure of 1 atm. In all cases, measurements proceeded from the highest temperature (673 K) to the lowest temperature (294 K) and were checked for reversibility by returning the system to the highest temperature and comparing the signal to the initial spectrum for that series. For signal averaging purposes, and to ensure attainment of a steady state condition, measurements at each temperature/pressure combination were made until three spectra containing indistinguishable white line intensities were obtained.

XAS Data Analysis. Data processing and analysis was conducted using the IFEFFIT package.[83] Quantitative XANES analysis relies on accurate energy assignment to each data point, and it is important to ensure that the energy scale is the same for all data. For that purpose, the reference Pt foil spectra measured simultaneously with the samples were alligned for all of the raw data, guaranteeing a consistent energy scale. The data were then merged and normalized by the edge-step for subsequent XANES analysis. To analyze the EXAFS data, we aligned the data together using the first inflection point in their spectra. This procedure was chosen in order to minimize the dependence of the results on the variations in the photoelectron energy origin that changes significantly, depending on the environmental condition used. Following the alignment, the smooth atomic background function was subtracted from the edge-step normalized data. The resultant k^2-weighted $\chi(k)$ function was fit in R-space using the Artemis program[84] (Supporting Information). The photoelectron scattering amplitudes and phases used in the fits were calculated with FEFF6[85] using a model structure of bulk fcc Pt.

In analyzing the temperature-dependent changes in the Pt clusters under each atmosphere at the highest at lowest temperatures (Figures 2−4), the CNs, bond lengths, and total bond length disorders were obtained using a multiple data set fitting scheme. In this scheme, each parameter was allowed to vary independently and the photoelectron energy origin was constrained to be the same for all clusters. The latter constraint is justifiable because the data are for EXAFS analysis, and the first inflection point on the absorption edge is at the same position for all data. A correction for a possible anharmonic term (the third cumulant) in the effective M−M pair potential was included in the model. For the room temperature data, the best fit values of the third cumulant were consistent with zero and were subsequently dropped to minimize the number of free parameters used in the fitting. To estimate the dynamic contribution to the total disorder, we used data available for similar size clusters (1.1 nm) of Pt/γ-Al_2O_3 measured under He.[9] This "zero coverage" proxy value was only used for our strain calculations, and we describe the details and consequences of this assumption in the discussion.

ΔXANES Data Analysis. The data were aligned in absolute energy as described above. We have chosen to use the 400 ppm at 673 K data for each gas as a reference spectrum for subtraction of all other spectra acquired at the same partial pressure (*e.g.*, Figure 5). All ΔXANES spectra were calculated by taking the spectra to be compared and interpolating the region

of comparison (11 523 to 11 605 eV) to a uniform grid of 2000 points and then subtracting the temperature-dependent spectra from the reference spectra using OriginPro software (OriginLab, Northampton, MA). Extrapolation to a uniform grid and alignment of the data using the Pt foils was found to be crucial to the analysis. A slight change in the energy between the spectra analyzed using ΔXANES can result in large errors because of the rapid intensity change that occurs at the adsorption edge. For both gases, the ΔXANES spectra were piecewise integrated to determine the area of each of the two resultant peaks (plotted in Figure 6). The first peak was integrated over the range 11 549 to 11 567 eV, while the second peak was integrated from 11 567 to 11 582 eV. These values were chosen based on the average position of the inflection points in the ΔXANES spectra. Other authors have reported using only the second peak to correlate coverage with the integrated intensity.[78] We, however, found that similar trends were obtained regardless of whether the integrated intensity of one peak or the absolute sum of both integrated peaks was used. We have, therefore, chosen to report the latter as it provides lower statistical uncertainties.

Fitting of the ΔXANES to a theoretical model (eq 10, *vide infra*) was done using OriginPro and defining all values except the heat of adsorption and a scaling constant related to the coverage. Defined values were either theoretically or experimentally determined. During the fitting procedure, the scaling constant was allowed to vary independent of adsorbate partial pressure while the heat of adsorption was constrained to be identical for the three partial pressures investigated.

Conflict of Interest: The authors declare no competing financial interest.

Acknowledgment. The authors would like to thank R. Vasić, A. Yevick, and C. Cooper for their help with the XAS data collection and processing. We would also like to thank W. Schneider for some insightful discussions. This work was sponsored in part by a grant from the U.S. Department of Energy (DE-FG02-03ER15476). Experiments were carried out in part at the Frederick Seitz Materials Research Laboratory Central Facilities, University of Illinois, which are partially supported by the U.S. Department of Energy under Grants DE-FG02-07ER46453 and DE-FG02-07ER46471. Research was also carried out at the National Synchrotron Light Source (NSLS) at Brookhaven National Laboratory. Use of the NSLS was supported by the U.S. Department of Energy, Office of Science, Office of Basic Energy Sciences, under Contract No. DE-AC02-98CH10886. Beamline X19A at the NSLS is supported in part by the Synchrotron Catalysis Consortium, U.S. Department of Energy Grant No DE-FG02-05ER15688.

Supporting Information Available: Additional microscopy images, XAS fits/results, tabulated values for graphs, and information on the coverage fitting model are provided in the Supporting Information. This material is available free of charge *via* the Internet at http://pubs.acs.org.

REFERENCES AND NOTES

1. Levenspiel, O. *Chemical Reaction Engineering*; 2nd ed.; John Wiley & Sons: New York, 1972.
2. Scarano, D.; Bordiga, S.; Lamberti, C.; Ricchiardi, G.; Bertarione, S.; Spoto, G. Hydrogen Adsorption and Spillover Effects on H-Y and Pd-Containing Y Zeolites an Experimental and Theoretical Investigation. *Appl. Catal., A* **2006**, *307*, 3–12.
3. Smith, J. M.; Van Ness, H. C. *Introduction to Chemical Engineering Thermodynamics*; 3rd ed.; McGraw-Hill Book Company: New York, 1975.
4. Diemant, T.; Zhao, Z.; Rauscher, H.; Bansmann, J.; Behm, R. J. Interaction of CO with Planar Au/TiO_2 Model Catalysts at Elevated Pressures. *Top. Catal.* **2007**, *44*, 83–93.
5. Somorjai, G. A.; Park, J. Y. Colloid Science of Metal Nanoparticle Catalysts in 2D and 3D Structures, Challenges of Nucleation, Growth, Composition, Particle Shape, Size Control and Their Influence on Activity and Selectivity. *Top. Catal.* **2008**, *49*, 126–135.
6. Li, Y.; Somorjai, G. A. Nanoscale Advances in Catalysis and Energy Applications. *Nano Lett.* **2010**, *10*, 2289–2295.
7. Rodriguez, J. A.; Goodman, D. W. High-Pressure Catalytic Reactions over Single-Crystal Metal Surfaces. *Surf. Sci. Rep.* **1991**, *14*, 1–107.
8. Small, M. W.; Sanchez, S. I.; Menard, L. D.; Kang, J. H.; Frenkel, A. I.; Nuzzo, R. G. The Atomic Structural Dynamics of γ-Al_2O_3 Supported Ir−Pt Nanocluster Catalysts Prepared from a Bimetallic Molecular Precursor: A Study Using Aberration-Corrected Electron Microscopy and X-ray Absorption Spectroscopy. *J. Am. Chem. Soc.* **2011**, *133*, 3582–3591.
9. Sanchez, S. I.; Menard, L. D.; Bram, A.; Kang, J. H.; Small, M. W.; Nuzzo, R. G.; Frenkel, A. I. The Emergence of Nonbulk Properties in Supported Metal Clusters: Negative Thermal Expansion and Atomic Disorder in Pt Nanoclusters Supported on γ-Al_2O_3. *J. Am. Chem. Soc.* **2009**, *131*, 7040–7054.
10. Zhou, M.; Zhang, A.; Dai, Z.; Feng, Y. P.; Zhang, C. Strain-Enhanced Stabilization and Catalytic Activity of Metal Nanoclusters on Graphene. *J. Phys. Chem. C* **2010**, *114*, 16541–16546.
11. Mavrikakis, M.; Hammer, B.; Norskov, J. K. Effect of Strain on the Reactivity of Metal Surfaces. *Phys. Rev. Lett.* **1998**, *81*, 2819–2822.
12. Strasser, P.; Koh, S.; Anniyev, T.; Greeley, J.; More, K.; Yu, C.; Liu, Z.; Kaya, S.; Nordlund, D.; Ogasawara, H.; *et al.* Lattice-Strain Control of the Activity in Dealloyed Core−Shell Fuel Cell Catalysts. *Nat. Chem.* **2010**, *2*, 454–460.
13. Hansen, P. L.; Wagner, J. B.; Helveg, S.; Rostrup-Nielsen, J. R.; Clausen, B. S.; Topsoe, H. Atom-Resolved Imaging of Dynamic Shape Changes in Supported Copper Nanocrystals. *Science* **2002**, *295*, 2053–2055.
14. Uner, D.; Uner, M. Adsorption Calorimetry in Supported Catalyst Characterization: Adsorption Structure Sensitivity on Pt/γ-Al_2O_3. *Thermochim. Acta* **2005**, *434*, 107–112.
15. Dulaurent, O.; Bianchi, D. Adsorption Isobars for CO on a Pt/Al_2O_3 Catalyst at High Temperatures Using FTIR Spectroscopy: Isosteric Heat of Adsorption and Adsorption Model. *Appl. Catal., A* **2000**, *196*, 271–280.
16. Bourane, A.; Dulaurent, O.; Salasc, S.; Sarda, C.; Bouly, C.; Bianchi, D. Heats of Adsorption of Linear NO Species on a Pt/Al_2O_3 Catalyst Using *In Situ* Infrared Spectroscopy under Adsorption Equilibrium. *J. Catal.* **2001**, *204*, 77–88.
17. Chen, H.-W.; White, J. M. TPD of Deuterium Spillover on Pt/Al_2O_3. *J. Mol. Catal.* **1986**, *35*, 355–364.
18. Guo, N.; Fingland, B. R.; Williams, W. D.; Kispersky, V. F.; Jelic, J.; Delgass, W. N.; Ribeiro, F. H.; Meyer, R. J.; Miller, J. T. Determination of CO, H_2O and H_2 Coverage by XANES and EXAFS on Pt and Au during Water Gas Shift Reaction. *Phys. Chem. Chem. Phys.* **2010**, *12*, 5678–5693.
19. Singh, J.; Tromp, M.; Safonova, O. V.; Glatzel, P.; Van Bokhoven, J. A. *In Situ* XAS with High-Energy Resolution: The Changing Structure of Platinum during the Oxidation of Carbon Monoxide. *Catal. Today* **2009**, *145*, 300–306.
20. Oudenhuijzen, M. K.; Van Bokhoven, J. A.; Miller, J. T.; Ramaker, D. E.; Koningsberger, D. C. Three-Site Model for Hydrogen Adsorption on Supported Platinum Particles: Influence of Support Ionicity and Particle Size on the Hydrogen Coverage. *J. Am. Chem. Soc.* **2005**, *127*, 1530–1540.
21. Vaarkamp, M.; Miller, J. T.; Modica, F. S.; Koningsberger, D. C. On the Relation between Particle Morphology, Structure of the Metal−Support Interface, and Catalytic Properties of Pt/γ-Al_2O_3. *J. Catal.* **1996**, *163*, 294–305.
22. Alexeev, O.; Kim, D.-W.; Graham, G. W.; Shelef, M.; Gates, B. C. Temperature-Programmed Desorption of Hydrogen from Platinum Particles on γ-Al_2O_3: Evidence of Platinum-Catalyzed Dehydroxylation of γ-Al_2O_3. *J. Catal.* **1999**, *185*, 170–181.
23. Ahmed, F.; Alam, M. K.; Suzuki, A.; Koyama, M.; Tsuboi, H.; Hatakeyama, N.; Endou, A.; Takaba, H.; Del Carpio, C. A.; Kubo, M.; *et al.* Dynamics of Hydrogen Spillover on Pt/γ-Al_2O_3 Catalyst Surface: A Quantum Chemical Molecular Dynamics Study. *J. Phys. Chem. C* **2009**, *113*, 15676–15683.

24. Safonova, O. V.; Tromp, M.; Van Bokhoven, J. A.; de Groot, F. M. F.; Evans, J.; Glatzel, P. Identification of CO Adsorption Sites in Supported Pt Catalysts Using High-Energy-Resolution Fluorescence Detection X-ray Spectroscopy. *J. Phys. Chem. B* **2006**, *110*, 16162–16164.
25. Digne, M.; Sautet, P.; Raybaud, P.; Euzen, P.; Toulhoat, H. Use of DFT To Achieve a Rational Understanding of Acid-Basic Properties of γ-Alumina Surfaces. *J. Catal.* **2004**, *226*, 54–68.
26. Stakheev, A. Y.; Zhang, Y.; Ivanov, A. V.; Baeva, G. N.; Ramaker, D. E.; Koningsberger, D. C. Separation of Geometric and Electronic Effects of the Support on the CO and H_2 Chemisorption Properties of Supported Pt Particles: The Effects of Ionicity in Modified Alumina Supports. *J. Phys. Chem. C* **2007**, *111*, 3938–3948.
27. Schneider, S.; Bazin, D.; Meunier, G.; Noirot, R.; Capelle, M.; Garin, F.; Maire, G. An EXAFS Study of the Interaction of Different Reactant Gases over Nanometer Scale Pt Clusters Deposited on γ-Al_2O_3. *Catal. Lett.* **2001**, *71*, 155–162.
28. Vila, F.; Rehr, J. J.; Kas, J.; Nuzzo, R. G.; Frenkel, A. I. Dynamic Structure in Supported Pt Nanoclusters: Real-Time Density Functional Theory and X-ray Spectroscopy Simulations. *Phys. Rev. B* **2008**, *78*, 121404(R)/121401–121404.
29. Frenkel, A. I.; Hills, C. W.; Nuzzo, R. G. A View from the Inside: Complexity in the Atomic Scale Ordering of Supported Metal Nanoparticles. *J. Phys. Chem. B* **2001**, *105*, 15689–12703.
30. Rioux, R. M.; Song, H.; Grass, M.; Habas, S.; Niesz, K.; Hoefelmeyer, J. D.; Yang, P.; Somorjai, G. A. Monodisperse Platinum Nanoparticles of Well-Defined Shape: Synthesis, Characterization, Catalytic Properties and Future Prospects. *Top. Catal.* **2006**, *39*, 167–174.
31. Huang, W. J.; Sun, R.; Tao, J.; Menard, L. D.; Nuzzo, R. G.; Zuo, J. M. Coordination-Dependent Surface Atomic Contraction in Nanocrystals Revealed by Coherent Diffraction. *Nat. Mater.* **2008**, *7*, 308–313.
32. Chen, J.; Lim, B.; Lee, E. P.; Xia, Y. Shape-Controlled Synthesis of Platinum Nanocrystals for Catalytic and Electrocatalytic Applications. *Nano Today* **2009**, *4*, 81–95.
33. Rupprechter, G.; Freund, H.-J. Adsorbate-Induced Restructuring and Pressure-Dependent Adsorption on Metal Nanoparticles Studied by Electron Microscopy and Sum Frequency Generation Spectroscopy. *Top. Catal.* **2001**, *14*, 3–14.
34. Hu, C. H.; Chizallet, C.; Mager-Maury, C.; Corral-Valero, M.; Sautet, P.; Toulhoat, H.; Raybaud, P. Modulation of Catalyst Particle Structure upon Support Hydroxylation: *Ab Initio* Insights into Pd_{13} and Pt_{13}/γ-Al_2O_3. *J. Catal.* **2010**, *274*, 99–110.
35. Cuenya, B. R.; Frenkel, A. I.; Mostafa, S.; Behafarid, F.; Croy, J. R.; Ono, L. K.; Wang, Q. Anomalous Lattice Dynamics and Thermal Properties of Supported Size- and Shape-Selected Pt Nanoparticles. *Phys. Rev. B* **2010**, *82*, 155450–155451/155458.
36. Cuenya, B. R.; Croy, J. R.; Mostafa, S.; Behafarid, F.; Li, L.; Zhang, Z.; Yang, J. C.; Wang, Q.; Frenkel, A. I. Solving the Structure of Size-Selected Pt Nanocatalysts Synthesized by Inverse Micelle Encapsulation. *J. Am. Chem. Soc.* **2010**, *132*, 8747–8756.
37. Paredis, K.; Ono, L. K.; Mostafa, S.; Li, L.; Zhang, Z.; Yang, J. C.; Barrio, L.; Frenkel, A. I.; Cuenya, B. R. Structure, Chemical Composition, and Reactivity Correlations during the *In Situ* Oxidation of 2-Propanol. *J. Am. Chem. Soc.* **2011**, *133*, 6728–6735.
38. Yevick, A.; Frenkel, A. I. Effects of Surface Disorer on EXAFS Modeling of Metallic Clusters. *Phys. Rev. B* **2010**, *81*, 115451/115451–115457.
39. Mays, C. W.; Vermaak, J. S.; Kuhlmann-Wilsdorf, D. On Surface Stress and Surface Tension. *Surf. Sci.* **1968**, *12*, 134–140.
40. Vermaak, J. S.; Mays, C. W.; Kuhlmann-Wilsdorf, D. On Surface Stress and Surface Tension. *Surf. Sci.* **1968**, *12*, 128–133.
41. Tomanek, D.; Mukherjee, S.; Bennemann, K. H. Simple Theory for the Electronic and Atomic Structure of Small Clusters. *Phys. Rev. B* **1983**, *28*, 665–673.
42. Kwak, J. H.; Hu, J.; Mei, D.; Yi, C.-W.; Kim, D. H.; Peden, C. H. F.; Allard, L. F.; Szanyi, J. Coordinatively Unsaturated Al^{3+} Centers as Binding Sites for Active Catalyst Phases of Platinum on γ-Al_2O_3. *Science* **2009**, *325*, 1670–1673.
43. Gontard, L. C.; Dunin-Borkowski, R. E.; Gass, M. H.; Bleloch, A. L.; Ozkaya, D. Three-Dimensional Shapes and Structures of Lamellar-Twinned FCC Nanoparticles Using ADF STEM. *J. Electron. Microsc.* **2009**, *58*, 167–174.
44. Gontard, L. C.; Dunin-Borkowski, R. E.; Ozkaya, D. Three-Dimensional Shapes and Spatial Distributions of Pt and PtCr Catalyst Nanoparticles on Carbon Black. *J. Microsc.* **2008**, *232*, 248–259.
45. Sonstrom, P.; Baumer, M. Supported Colloidal Nanoparticles in Heterogeneous Gas Phase Catalysis: On the Way to Tailored Catalysts. *Phys. Chem. Chem. Phys.* **2011**, *13*, 19270–19284.
46. Wang, L.-L.; Khare, S. V.; Chirita, V.; Johnson, D. D.; Rockett, A. A.; Frenkel, A. I.; Mack, N. H.; Nuzzo, R. G. Origin of Bulklike Structure and Bond Length Disorder of Pt_{37} and Pt_6Ru_{31} Clusters on Carbon: Comparison of Theory and Experiment. *J. Am. Chem. Soc.* **2006**, *128*, 131–142.
47. Tao, F.; Dag, S.; Wang, L.-W.; Liu, Z.; Butcher, D. R.; Bluhm, H.; Salmeron, M.; Somorjai, G. A. Break-up of Stepped Platinum Catalyst Surfaces by High CO Coverage. *Science* **2010**, *327*, 850–853.
48. Somorjai, G. A. The Surface Science of Heterogeneous Catalysis. *Surf. Sci.* **1994**, *299*, 849–866.
49. Gates, B. C. *Catalytic Chemistry*; John Wiley & Sons, Inc.: New York, 1992.
50. Imbihl, R.; Ertl, G. Oscillatory Kinetics in Heterogeneous Catalysis. *Chem. Rev.* **1995**, *95*, 697–733.
51. Kang, J. H.; Menard, L. D.; Nuzzo, R. G.; Frenkel, A. I. Unusual Non-bulk Properties in Nanoscale Materials: Thermal Metal−Metal Bond Contraction of γ-Al_2O_3-Supported Pt Catalysts. *J. Am. Chem. Soc.* **2006**, *128*, 12068–12069.
52. Wang, L.-L.; Johnson, D. D. Shear Instabilitities in Metallic Nanoparticles: Hydrogen-Stabilized Structure of Pt_{37} on Carbon. *J. Am. Chem. Soc.* **2007**, *129*, 3658–3664.
53. Kobayashi, H.; Yamauchi, M.; Kitagawa, H.; Kubota, Y.; Kato, K.; Takata, M. Atomic-Level Pd−Pt Alloying and Largely Enhanced Hydrogen-Storage Capacity in Bimetallic Nanoparticles Reconstructed from Core/Shell Structure by a Process of Hydrogen Absorption/Desorption. *J. Am. Chem. Soc.* **2010**, *132*, 5576–5577.
54. Tao, F.; Grass, M. E.; Zhang, Y.; Butcher, D. R.; Renzas, J. R.; Liu, Z.; Chung, J. Y.; Mun, B. S.; Salmeron, M.; Somorjai, G. A. Reaction-Driven Restructuring of Rh−Pd and Pt−Pd Core−Shell Nanoparticles. *Science* **2008**, *322*, 932–934.
55. Vannice, M. A.; Hasselbring, L. C.; Sen, B. Direct Measurements of Heats of Adsorption on Platinum Catalysts. *J. Catal.* **1985**, *95*, 57–70.
56. Sen, B.; Vannice, M. A. The Influence of Platinum Crystallite Size on H_2 and CO Heats of Adsorption and CO Hydrogenation. *J. Catal.* **1991**, *130*, 9–20.
57. Pearson, R. G. Absolute Electronegativity and Hardness: Application to Inorganic Chemistry. *Inorg. Chem.* **1988**, *27*, 734–740.
58. Chen, L.; Chen, B.; Zhou, C.; Wu, J.; Forrey, R. C.; Cheng, H. Influence of CO Poisoning on Hydrogen Chemisorption onto a Pt_6 Cluster. *J. Phys. Chem. C* **2008**, *112*, 13937–13942.
59. McKenna, K. P.; Shluger, A. L. Shaping the Morphology of Gold Nanoparticles by CO Adsorption. *J. Phys. Chem. C* **2007**, *111*, 18848–18852.
60. Campbell, C. T. Ultrathin Metal Films and Particles on Oxide Surfaces: Structural, Electronic and Chemisorptive Properties. *Surf. Sci. Rep.* **1997**, *27*, 1–111.
61. Vaarkamp, M.; Modica, F. S.; Miller, J. T.; Koningsberger, D. C. Influence of Hydrogen Pretreatment on the Structure of the Metal−Support Interface in Pt/Zeolite Catalysts. *J. Catal.* **1993**, *144*, 611–626.
62. Samant, M. G.; Boudart, M. Support Effects on Electronic Structure of Platinum Clusters in Y Zeolite. *J. Phys. Chem.* **1991**, *95*, 4070–4074.

63. Van Bokhoven, J. A.; Roest, A. L.; Koningsberger, D. C.; Miller, J. T.; Nachtegaal, G. H.; Kentgens, A. P. M. Changes in Structural and Electronic Properties of the Zeolite Framework Induced by Extraframework Al and La in H-USY and La(*x*)NaY: A ^{29}Si and ^{27}Al MAS NMR and ^{27}Al MQ MAS NMR Study. *J. Phys. Chem. B* **2000**, *104*, 6743–6754.
64. Nilekar, A. U.; Xu, Y.; Zhang, J.; Vukmirovic, M. B.; Sasaki, K.; Adzic, R. R.; Mavrikakis, M. Bimetallic and Ternary Alloys for Improved Oxygen Reduction Catalysis. *Top. Catal.* **2007**, *46*, 276–284.
65. Sanchez, S. I.; Small, M. W.; Zuo, J. M.; Nuzzo, R. G. Structural Characterization of Pt−Pd and Pd−Pt Core−Shell Nanoclusters at Atomic Resolution. *J. Am. Chem. Soc.* **2009**, *131*, 8683–8689.
66. Ertl, G.; Neumann, M.; Streit, K. M. Chemisorption of CO on the Pt(111) Surface. *Surf. Sci.* **1977**, *64*, 393–410.
67. Ji, Y.; Koot, V.; van der Eerden, A. M. J.; Weckhuysen, B. M.; Koningsberger, D. C.; Ramaker, D. E. A Three-Site Langmuir Adsorption Model To Elucidate the Temperature, Pressure, and Support Dependence of the Hydrogen Coverage on Supported Pt Particles. *J. Catal.* **2007**, *245*, 415–427.
68. Luo, J. S.; Tobin, R. G.; Lambert, D. K.; Fisher, G. B.; DiMaggio, C. L. CO Adsorption Site Occupation on Pt(335): A Quantitative Investigation Using TPD and EELS. *Surf. Sci.* **1992**, *274*, 53–62.
69. Frenkel, A. I.; Stern, E. A.; Voronel, A.; Heald, S. M. Lattice Strains in Disordered Mixed Salts. *Solid State Commun.* **1996**, *99*, 67–71.
70. Tchernatinsky, A.; Halley, J. W. Relativistic Tight-Binding Model: Application to Pt Surfaces. *Phys. Rev. B* **2011**, *83*, 205431.
71. Aray, Y.; Rodriguez, J.; Vega, D. Topology of the Electron Density and Cohesive Energy of the Face-Centered Cubic Transition Metals. *J. Phys. Chem. B* **2000**, *104*, 4608–4612.
72. Qi, W. H.; Wang, M. P. Size Effect on the Cohesive Energy of Nanoparticle. *J. Mater. Sci. Lett.* **2002**, *21*, 1743–1745.
73. Davenport, J. W.; Watson, R. E.; Weinert, M. Cohesive and Structural Energies for the 5d Elements, Lu through Au. *Phys. Scr.* **1985**, *32*, 425–428.
74. Hill, T. L. A Different Approach to Nanothermodynamics. *Nano Lett.* **2001**, *1*, 273–275.
75. Abe, S.; Rajagopal, A. K. Scaling Relations in Equilibrium Nonextensive Thermostatistics. *Phys. Lett. A* **2005**, *337*, 292–295.
76. Savargaonkar, N.; Uner, D.; Pruski, M.; King, T. S. Kinetics of Hydrogen Adsorption and Desorption on Silica-Supported Pt, Rh, and Ru Catalysts Studied by Solid State ^{1}H NMR. *Langmuir* **2002**, *18*, 4005–4009.
77. Kubota, T.; Asakura, K.; Iwasawa, Y. Quantitative Analysis of Hydrogen Adsorbed on Pt Particles on SiO_2 in the Presence of Coadsorbed CO by Means of L_3-Edge X-ray Absorption Near-Edge Structure Spectroscopy. *Catal. Lett.* **1997**, *46*, 141–144.
78. Asakura, K.; Kubota, T.; Chun, W.-J.; Iwasawa, Y.; Ohtani, K.; Fujikawa, T. Pt L_3-Edge XANES Studies about the Hydrogen Adsorption on Small Pt Particles. *J. Synchrotron Radiat.* **1999**, *6*, 439–441.
79. Kubota, T.; Asakura, K.; Ichikuni, N.; Iwasawa, Y. A New Method for Quantitative Characterization of Adsorbed Hydrogen on Pt Particles by Means of Pt L-Edge XANES. *Chem. Phys. Lett.* **1996**, *256*, 445–448.
80. Derrouiche, S.; Bianchi, D. Heats of Adsorption Using Temperature Programmed Adsorption Equilibrium: Application to the Adsorption of CO on Cu/Al_2O_3 and H_2 on Pt/Al_2O_3. *Langmuir* **2004**, *20*, 4489–4497.
81. Allian, A. D.; Takanabe, K.; Fujdala, K. L.; Hao, X.; Truex, T. J.; Cai, J.; Buda, C.; Neurock, M.; Iglesia, E. Chemisorption of CO and Mechanism of CO Oxidation on Supported Platinum Nanoclusters. *J. Am. Chem. Soc.* **2011**, *133*, 4498–4517.
82. Sanchez, S. I.; Small, M. W.; Sivaramakrishnan, S.; Wen, J.-G.; Zuo, J. M.; Nuzzo, R. G. Visualizing Materials Chemistry at Atomic Resolution. *Anal. Chem.* **2010**, *82*, 2599–2607.
83. Newville, M. IFEFFIT: Interactive XAFS Analysis and FEFF Fitting. *J. Synchrotron Radiat.* **2001**, *8*, 322–324.
84. Ravel, B.; Newville, M. ATHENA, ARTEMIS, HEPHAESTUS: Data Analysis for X-ray Absorption Spectroscoopy Using IFEFFIT. *J. Synchrotron Radiat.* **2005**, *12*, 537–541.
85. Zabinsky, S. I.; Rehr, J. J.; Ankudinov, A.; Albers, R. C.; Eller, M. J. Multiple-Scattering Calculations of X-ray-Absorption Spectra. *Phys. Rev. B* **1995**, *52*, 2995–3009.